Quantum size effect across semiconductor-to-metal phase transition in vanadium dioxide thin films

G.R. Khan, B.A. Bhat

Nanotechnology Research Lab, Department of Physics, National Institute of Technology, Srinagar 19006, Kashmir, India
E-mail: grkhan786@gmail.com

Published in Micro & Nano Letters; Received on 19th May 2015; Revised on 22nd July 2015; Accepted on 23rd July 2015

The phase transition temperature of vanadium dioxide (VO_2) thin films shifts to the vicinity of room temperature by reducing the dimensions from microscale to nanoscale without the use of any dopant. This quantum size effect elucidated by studying the structural, optical and electrical properties of nanothin and microthin films of VO_2 across their semiconductor–metal phase transitions has been demonstrated in this reported work. The films fabricated on glass substrates via the inorganic sol–gel route were characterised by Rutherford backscattering spectrometry (RBS), X-ray diffractometery, scanning electron microscopy, ultraviolet–visible spectroscopy and the four-probe method. The RBS results estimate a layer thickness of 15 and 291 nm for nanothin and microthin films, respectively. The films were polycrystalline in their nature of [011] orientation with regular and irregular crystallites of a cuboidal surface morphology. Estimation of crystallite size revealed that nanothin films attain poor crystallinity as compared with microthin films. The blue shift was observed in nanothin films from microthin films as maximum absorption occurred at wavelengths of 360 and 443 nm, respectively. Optical bandgaps of 2.3 and 1.87 eV were found for nanothin and microthin films, respectively. Depletion in metal-to-semiconductor and semiconductor-to-metal transition temperatures were experienced from higher temperature regimes of 341 and 335 K for microthin films to lower temperature regimes of 319 and 305 K for nanothin films, respectively.

1. Introduction: The quantum size effect becomes predominant when matter miniaturises to the nanoscale thereby drastically affecting the optical, electrical and structural behaviour of materials. The cause of these radical changes stem from exciting quantum and surface phenomena that matter exhibits at the nanoscale where quantisation of energy for the electrons becomes extremely relevant.

Vanadium dioxide (VO_2) has been one of the most studied correlated electron systems that undergoes a temperature-driven first-order reversible semiconductor-to-metal transition (SMT) at a temperatures of about 68°C. It has closer propinquity to ambient temperature than that of any other reported compound with thermochromic behaviour [1]. During phase transition dynamics, the crystal structure of VO_2 transforms from low-temperature monoclinic phase (M_1, P_{21}/c) into high-temperature tetragonal rutile phase (R, P_{42}/mnm) [2]. The foremost characteristics of this structural phase transition consists of two distinct features: dimerisation of V–V chains along the rutile *c*-axis, and anti-ferroelectric distortion of V–V pairs towards the apex oxygen atoms [3]. The metal–insulator transition in VO_2 is referred to as a simultaneous Mott–Peierls transition due to an electronic Mott mechanism and thermal Peierls transition [4]. Above SMT, VO_2 exhibits metallic behaviour, whereas below SMT it demonstrates semiconducting behaviour [5–6].

The phase transition accompanied by an abrupt change in the electrical resistivity also undergoes rapid variations in its optical properties in the near-infrared region ranging between 0.8 and 2.2 μm [6]. Usually, single crystals get damaged due to thermal expansion across the phase transition during repeated thermal cycling but VO_2 thin films sustain damage all along the thermal cycling process. This has made it viable for a diverse range of applications like energy conserving coatings [7, 8], temperature sensors [9], thermo-optical switches [10], thermo-optical light modulators [11], energy storage media [12] and variable reflectance mirrors [13]. However, in most of the foregoing applications, it has become vital that the phase transition temperature of VO_2 thin films be reduced to near ambient. Enormous efforts have been made to shift the phase transition temperature to the proximity of room temperature. Elemental doping has been employed as an effective technique to modify the phase transition temperature of VO_2 thin films [12–19].

Doping with high-valent cations (Nb^{5+}, Ta^{5+}, W^{6+}, Mo^{6+}) generates donor-like defects that decrease the transition temperature, whereas doping with low-valent cations (Al^{3+}, Cr^{3+}, Fe^{3+}) generates acceptor-like defects that increase the transition temperature. As an example, W-doping in VO_2 thin films reduces the phase transition temperature to 45.15°C.

Devoid of doping, the semiconductor–metal phase transition temperatures of VO_2 thin films can be tuned to lower values by reducing the grain size of crystallites. The contour of the resistance–temperature hysteresis in the phase transition dynamics depends on the grain size of the crystallites. On the onehand, VO_2 crystals exhibit a marginal hysteresis width of <1°C, while on the other, VO_2 thin films depict hysteresis widths of the order of 10–15°C, and in nanofilms the hysteresis widths may grow even larger [20–24]. However, the fabrication of VO_2 stoichiometry thin films has not been a straightforward task because other vanadium oxides such as V_2O_3, V_3O_5 and V_2O_5 also produce stable structures in analogous conditions during VO_2 growth [25]. Therefore, to deposit VO_2 thin films on various substrates, many physical and chemical procedures have been reported such as sol–gel [26], chemical vapour deposition [27], anodic oxidation [28], magnetron sputtering [29] and laser ablation [30]. A comparative study of the properties of VO_2 thin films on different substrates demonstrates that local inhomogeneities, crystallite size and the distribution of crystallite size play a crucial role in the dynamics of the phase transition besides influencing the width and slope of its hysteresis loop [31].

As a recompense of high purity, superior homogeneity and excellent stoichiometry, the sol–gel process has emerged as an approach of paramount importance to deposit VO_2 thin films on a substrate [26, 32]. However, the organic sol–gel method relies on remarkably expensive and typically unstable vanadium alkoxides as precursors. Evading this drawback, the inorganic sol–gel route has been employed for the first time, to the best knowledge of the authors,

using vanadium pentaoxide (V_2O_5) powder and hydrogen peroxide (H_2O_2) as primary precursors.

In this Letter, we report a comprehensive study of nanothin films and microthin films of VO_2 based on analytic evaluation via the measurement of the structural, optical and electrical properties across their semiconductor-to-metal and metal-to-semiconductor transitions to elucidate how phase transition temperature plunges towards room temperature by plummeting its dimensions from microscale to nanoscale.

Nanothin and microthin VO_2 films were grown on amorphous glass substrates using V_2O_5 powder and H_2O_2 as starting precursors through the inorganic sol–gel process. No peaks corresponding to any impurity were established which specify that the films were of high phase purity, and no peaks corresponding to other oxides of vanadium were recognised which established that the main chemical composition of the films was homogeneous. Maximum energy absorption has been observed at wavelengths of 360 and 443 nm for nanothin and microthin films, respectively, which demonstrated the occurrence of a blue shift in nanothin films. Rutherford backscattering spectrometry (RBS) analysis estimated a thickness of VO_2 layers of 15 and 291 nm for nanothin films and microthin films, respectively.

A low phase transition temperature of about 319 K for VO_2 nanothin films compared with 341 K for microthin films has been realised. A broad transition with a large resistance–temperature hysteresis loop of 30 K was observed between the semiconductor-to-metal and metal-to-semiconductor transitions for nanothin films, whereas for microthin films, it was just 12 K. The optical bandgap widened from 1.87 eV for microthin to 2.30 eV for nanothin films.

2. Film fabrication: Films of assorted thickness were fabricated by dissolving 0.3 g of V_2O_5 (Sigma Aldrich, purity >99.9%) in 30 ml of 30% H_2O_2 solution (Sigma Aldrich) at room temperature amid vigorous stirring till a clear yellow solution was formed. The yellow solution was subsequently heated to 60°C with continuous stirring to evolve excess oxygen by the decomposition of H_2O_2 which right away transformed into a red-brown viscous gel. After aging for 24 h, the V_2O_5 gel was employed for coating of the thin films. The reaction mechanism is specified as follows [29]

$$V_2O_5 + 2H_2O_2 \rightarrow 2HVO_4 + H_2O \quad (1)$$

$$2HVO_4 + (n-1)H_2O \rightarrow V_2O_5 \cdot nH_2O + O_2 \quad (2)$$

The spin coater (ApexicIndia spinNXG-P1) was used to cast thin films on ultraclean high-quality glass substrates. Prior to deposition, the glass substrates were boiled in dilute sulphuric acid for 30 min followed by meticulous rinsing with ethanol, acetone and deionised water. Nanothin films of V_2O_5 gel were deposited on glass substrates by single coating at a spin rate of 6000 rpm for 30 s and dried up at 80°C for 20 min on a hotplate. Microthin films were fabricated by repeating the above-mentioned process ten times. These V_2O_5 films were crystallised and reduced to VO_2 by annealing at 450°C for 4 h in a mixture of argon (95%) and hydrogen (5%) inside a programmable tubular furnace (Nabertherm GmbH Tube furnace: RHTC80) with a heating and cooling rate of 3°C min^{-1}.

3. Characterisation: X-ray diffractometery (XRD) was performed to characterise the phase purity and analyse the crystal structure of the films by using a Bruker D8 Advance diffractometer (Cu-K_α radiation) at room temperature in the 2θ range of 20–70°. The optical measurements were carried out by means of an ultraviolet–visible (UV–Vis) spectrophotometer (Pharma Spec-1700, Shimadzu Corporation). The stoichiometry, thickness and uniformity of the thin films were explored by RBS with He^+ ions of energy 2 MeV. The surface morphology of the films was probed using a scanning electron microscope (MIRA II LMH, TESCAN). A standard four-probe setup fitted with a lakeshore temperature controller and a Keithley 2612A system sourcemeter was used to establish the temperature dependence of the resistivity of the films.

4. RBS studies: Since vanadium oxides do exhibit a wide range of stochiometries, RBS measurements with a simulation program (SIMNRA) were used to determine the thickness, composition and distribution of V and O elements in the vanadium oxide layers of the films. Fig. 1 depicts the experimental spectra along with the simulated RBS spectra of the nanothin and microthin VO_2 films. The O/V ratio for both films was 2, which falls within the simulation error range, thereby indicating the good stochiometries of both films.

The thickness of the VO_2 layers was found to be about 15 and 291 nm, respectively. The simulated results of films obtained from the SIMNRA program are summarised in Table 1. The RBS results reveal that no contamination was incorporated during the process of film deposition. The other elements displayed in the simulation Table are merely ingredients of the glass substrate.

5. XRD analysis: Fig. 2 displays the XRD pattern of the nanothin and microthin films. The diffraction peaks of both films can be indexed to a monoclinic symmetry of VO_2 (JCPDS Card No. 43–1051, space group $P2_1/c$). No peaks corresponding to any impurity were ascertained, which specify that the films were of high phase purity, and no peaks corresponding to other oxides of vanadium were identified, which confirmed that the main chemical composition of the films was homogeneous. As is

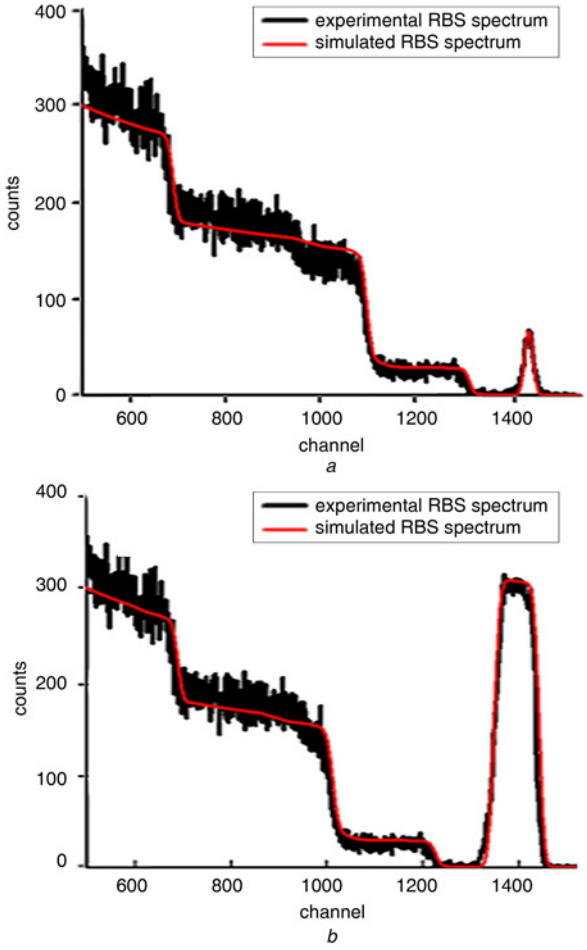

Figure 1 *Experimental and simulated RBS spectra of VO_2 films*
a Nanothin
b Microthin

doi: 10.1049/mnl.2015.0213

Table 1 Simulation results of nanothin and microthin VO_2 films

Film layer	Nanothin film		Microthin film	
	Thickness	composition	Thickness	composition
VO_2 film	15 nm	V = 0.333 O = 0.666	291 nm	V = 0.333 O = 0.666
glass substrate	5 µm	O = 0.600 Si = 0.250 B = 0.090 Na = 0.100 Al = 0.010 Ca = 0.030 Mg = 0.010	5 µm	O = 0.600 Si = 0.250 B = 0.090 Na = 0.100 Al = 0.010 Ca = 0.030 Mg = 0.010

clearly observable in the XRD patterns of both films, a strong peak appearing at 27.72° corresponds to VO_2 (011) reflection, and two low intensity peaks at 39.5° and 57.63° correspond to reflections from VO_2 (200) and VO_2 (220), respectively. In addition to these three peaks, the microthin films contain two more peaks at 44° and 55.5°, that can be assigned to reflections from the (210) and (211) planes, respectively. Despite the existence of other out-of-plane orientations, the high intensity peak (011) when compared with other peaks indicates that VO_2 prefers to align along (011) on glass substrate in view of the fact that the (011) plane has the low-energy plane of the monoclinic phase of VO_2 [30].

Table 2 shows the average crystal size (D), specific surface area (S) and microstrain (ε) estimated from the XRD analysis of the VO_2 thin films at the main intensity (011) peak. The average crystallite size was calculated from the Debye-Scherrer formula, $D = K\lambda/\beta\cos\theta$, and the specific surface area was found from the relationship, $S = 6/\rho D$, and the microstrain was estimated from the equation, $\varepsilon = \beta/4\tan\theta$, where K is the Scherer constant, λ is the wavelength of the Cu-K_α radiation, β is the full-width at half maximum of the XRD lines, θ is the Bragg diffraction angle and ρ is the material density [33]. It has been verified that nanothin films acquire poor crystalline with large strain as compared with microthin films. The poor crystallinity of nanothin films can be ascribed to the paucity of ample material available for the growth of nuclei following the nucleation of the monoclinic phase once films were cooled under sub-phase transition temperature post-annealing.

6. SEM investigations: Fig. 3 portrays the SEM micrographs of the VO_2 thin films. Uneven crystallites of exceedingly varying sizes were visibly apparent on the surface of nanothin films, whereas these were diverse sizes of cuboidal coiled crystallites veneer on

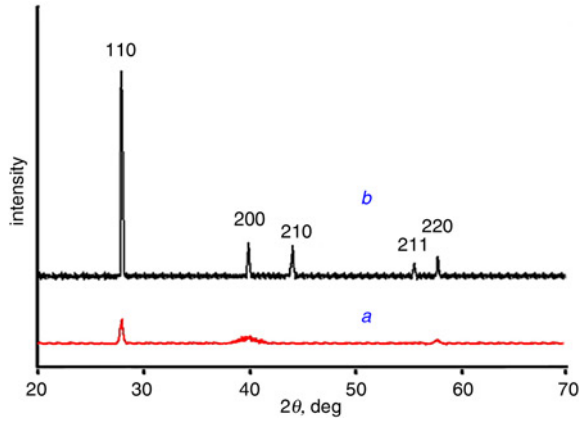

Figure 2 *XRD spectra of VO_2 films*
a Nanothin *b* Microthin

Table 2 Average crystal size (D), specific surface area (S) and microstrain (ε) estimated from XRD analysis of VO_2 thin films

VO_2 films	D, nm	S, m^2g^{-1}	$\varepsilon \times 10^{-4}$
nanothin	16	67	88
microthin	82	13	18

the microthin films. The range of grain size has grown wider in respect of nanothin films. Augmentation of dissimilar sized crystallites may be due to the heterogeneous nucleation of the semiconducting monoclinic phase of VO_2 during past-annealing cooling of the films to room temperature. The existence of asymmetrical sized crystallites in nanothin film loads to its inferior porosity with the minor grains acting as fillers wrapping the inter-granular space between the major ones. Furthermore, detectable tiny cracks develop on the surface of nanothin films. These fissures may have originated as a result of the contraction of gel during the annealing process due to the temperature gradient. The insets of the micrographs also show the histograms of the films plotted by measuring the distribution of grain sizes from their corresponding micrographs. The typical crystallite sizes determined from histograms by Lorentz curve fitting were reckoned to be 40.19 and 175.79 nm, respectively.

7. UV–Vis spectroscopy: Fig. 4 displays the UV–Vis absorption spectra of the VO_2 films. Maximum energy absorption has been observed to take place at wavelengths of 360 and 443 nm for nanothin and microthin films, respectively; thereby demonstrating

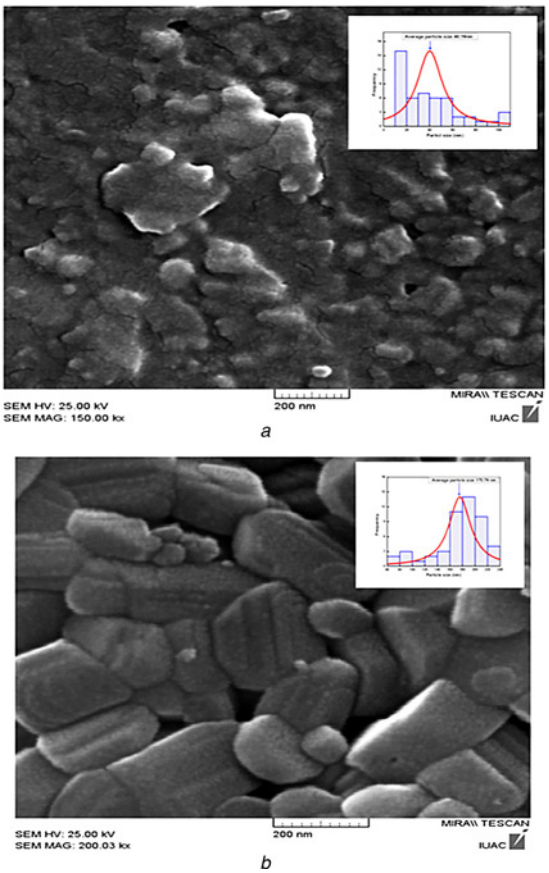

Figure 3 *SEM micrographs of VO_2 films*
a Nanothin
b Microthin
Insets show corresponding histograms

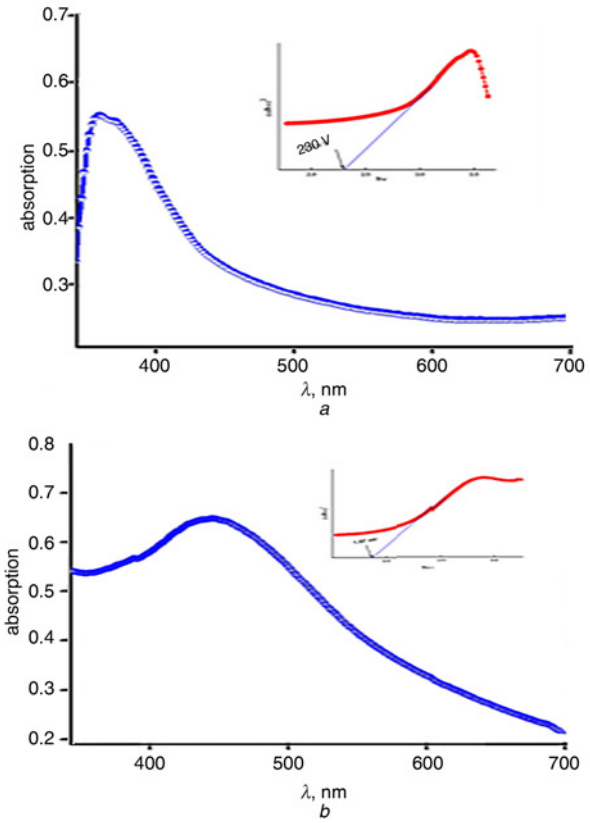

Figure 4 *UV–Vis absorption spectra of VO_2 films*
a Nanothin
b Microthin

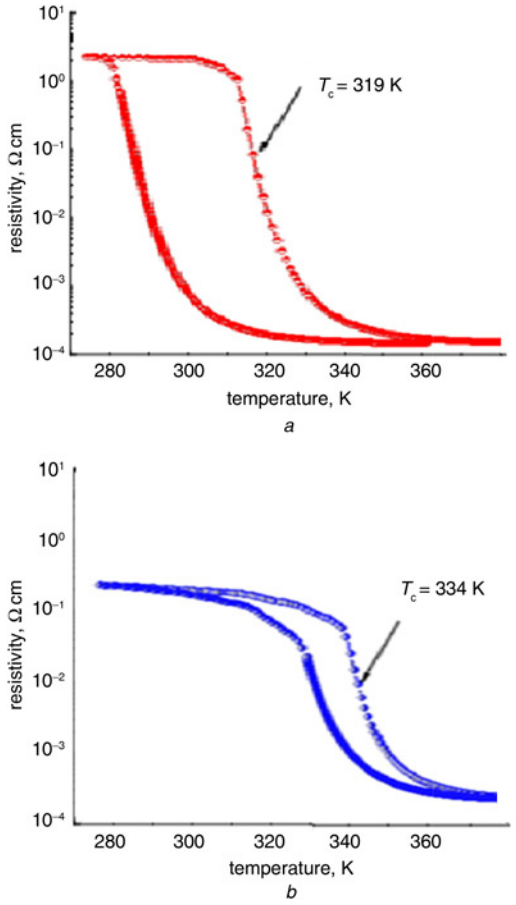

Figure 6 *Resistivity against temperature of VO_2 films*
a Nanothin
b Microthin

the occurrence of a blue shift in the nanothin films. The optical energy bandgap (E_g) of the films has been determined from the absorption spectra with the help of the Tauc relationship, $\alpha h\nu = A(h\nu - E_g)^n$, where α is the absorption coefficient, h is the Plank's constant, ν is the incident photon frequency, A is the transition probability dependent constant and n is the optical absorption related index having a value of 1/2 for the allowed direct bandgap semiconductor (VO_2) [33]. Tauc plots drawn for $(\alpha h\nu)^2$ against $h\nu$ provided an excellent linear relationship for both films. An energy band representation of the VO_2 semiconductor (monoclinic phase) is shown in Fig. 5. The electronic band structure comprised a lower occupied (O 2p) energy band and a system of upper energy bands. The upper band system was formed as a result of the anti-bonding of the (V 3d) orbital which consists of an occupied (V 3d) band positioned below the Fermi

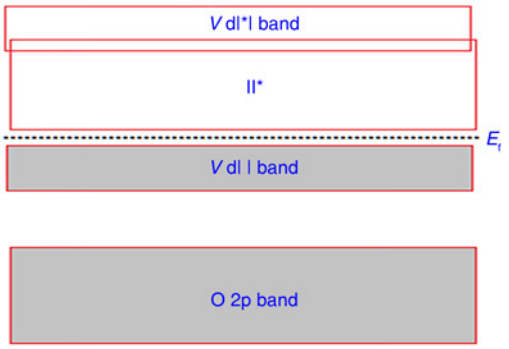

Figure 5 *Energy band representation of VO_2 semiconductor*

energy level, and an unoccupied (V 3d) band placed above the Fermi energy level. On the basis of this band structure, the optical transition can be segregated into two categories: 2p–3d inter-band transition and 3d–3d intra-band transition [34].

Using the Tauc equation, the values of the optical bandgap corresponding to 2p–3d inter-band transition for nanothin and microthin films were found to be 2.30 and 1.87 eV, respectively. The optical bandgap corresponding to 2p–3d inter-band transition for nanothin films was higher than the calculated values, whereas for microthin films it was in accordance with the theoretically calculated values [35]. This broadening of the bandgap in nanofilms can be expressed by the equation, $E_{Nano} = E + h^2/\{8\mu(d/2)\}^2 - 1.8e^2/\{\varepsilon(d/2)\}$ [36], where d is the average particle size, μ the reduced mass due to electron and hole effective masses and ε the semiconductor dielectric constant.

The second term on the right side of the equation represents the particle in a box like quantum localised energy and has $1/d^2$ dependence for both the electron and the hole. The third term represents the Coulomb energy with $1/d$ dependence. In the nanolimit ($d < 100$ nm), the second term of the equation dominates in comparison to the third term and thus explains the bandgap broadening in the nanothin film.

8. Four-probe scrutiny: VO_2 nanothin films and microthin films were evaluated for electrical properties by establishing their dependence of electrical resistivity on temperature using a standard four-probe method. The temperature of the films was primarily increased in steps from 280 to 380 K, and subsequently reduced to 280 K. Fig. 6 exhibits the electrical resistivity against temperature for the films. The phase transition behaviour of VO_2

doi: 10.1049/mnl.2015.0213

nanothin films differs from VO_2 microthin films. As is obvious from the graphs, metal-to-semiconductor and semiconductor-to-metal transitions undergo a paradigm shift to lower temperature values of 319 and 305 K for nanothin films from the higher temperature values of 341 and 335 K for microthin films, respectively. As a matter of fact, a broad transition with a large hysteresis as much as 30 K was observed between the semiconductor-to-metal and metal-to-semiconductor transitions for nanothin films, whereas for microthin films it was barely 12 K. It was also observed that the electrical resistivity in the semiconducting phase was higher in nanothin films in comparison to microthin films. The cause of the lowering of the phase transition in nanothin films may be due to an increased number of atoms distributed randomly at grain boundaries, resulting in a large surface and interface ratio. The rationale was that the smaller grain sizes damage the characteristic zigzag chains of V–V pairs that resulted in destabilisation of the low-temperature phase and lead to the decrease of the transition temperature. The lowering of the transition temperature in nanothin films can be understood with the help of the Mott-Hubbard system in which the U/W ratio, between the electron–electron Coulomb interaction (U) and the one-electron bandwidth (W), is an important parameter to control the properties; the system remains metallic to $U/W < 1$ and becomes insulating once $U/W > 1$ [37–43]. The sturdy spatial confinement of electronic wave functions in the VO_2 nanograin illustrates that electronic interaction U enhances as the average grain size diminishes. The larger value tends to stabilise the semiconducting phase in films, but at the same time W increases at a much faster rate as the thickness decreases, making U/W smaller for nanothin films compared with microthin films. This implies that the SMT was fairly likely to occur in nanothin films, thus being quite consistent with our experimental results. Moreover, the thermodynamic method based on the Laplace-Young equation predicts that the decrease in phase transition temperature can be expressed as, $\Delta T = T - T_r = C\alpha(2\gamma/r)$, where T and T_r are the phase transition temperatures of microcrystals and corresponding nanocrystal related to the size (r), respectively, C is the proportionality constant, α is the parameter related to the transition temperature and γ is the surface tension [44].

The broadening of the resistance–temperature hysteresis loop in the nanothin films can be due to meager potent defects that are characteristics of grain boundaries and grain size. The smaller the grain size, the fewer will be the potent defects and hence the broader will be the hysteresis loop as only fewer available potent defects can nucleate heterogeneous SMI transition [45]. The narrowing of the hysteresis loop with increasing the size of nanoparticles stands clearly verified in VO_2 [24]. Furthermore, poor interconnectivity due to gaps between nanocrystals can also be responsible for broad transition with a large hysteresis in nanothin films. This broadening of the hysteresis loop in crystalline nanothin films is well in accordance with the thermodynamical model [45].

9. Conclusion: VO_2 undergoes a temperature-driven first-order reversible SMT at a temperature of about 68°C. For many applications, the phase transition temperature of VO_2 thin films needs to be reduced to close to room temperature. This can be realised through the so-called quantum size effect by plunging the grain size of crystallites in the films to the nanoscale, which has been confirmed by the study of the structural, optical and electrical properties of nanothin and microthin films of VO_2 across their semiconductor-to-metal phase transitions.

Nanothin and microthin VO_2 films were grown on amorphous glass substrates using V_2O_5 powder and H_2O_2 as starting precursors by the inorganic sol–gel method for the first time. No peaks corresponding to any impurity were ascertained, which specifies that the films were of high phase purity, and no peaks corresponding to other oxides of vanadium were identified, which established that the main chemical composition of the films was homogeneous. Maximum energy absorption has been observed to take place at wavelengths of 360 and 443 nm for nanothin and microthin films, respectively, therein demonstrating the occurrence of a blue shift in nanothin films. RBS studies revealed a thickness of the VO_2 layer to be about 15 and 291 nm, respectively. The values of the optical bandgap for nanothin and microthin films were found to be 2.30 and 1.87 eV, respectively.

Here, low phase transition temperatures of 319 and 341 K have been demonstrated for VO_2 nanothin and microthin films, respectively. A broad transition with a large hysteresis of 30 and 12 K was observed between the SMT and MST for nanothin and microthin films, respectively. The prominent hysteresis and low SMT temperature leads to the restructuring of the monoclinic phase in the nanodimensions that have prospective application for thermo-coating, optical switching and bolometric applications. The broadening of the optical bandgap in the semiconducting phase noticed in crystalline VO_2 nanothin films was attributed to the quantum confinement effect.

10 References

[1] Warwick M.E., Binions R.: 'Advances in thermochromic vanadium dioxide films', *J. Mater. Chem. A*, 2014, **2**, p. 3275

[2] Hong W.K., Cha S.N., Sohn J.I., Kim J.M.: 'Metal-insulator phase transition in quasi-one-dimensional VO_2 structures', *J. Nanomaterials*, 2015, **501**, p. 538954

[3] Goodenough J.B.: 'The two components of the crystallographic transition in VO_2', *Solid State Chem.*, 1971, **3**, p. 490

[4] Eyert V.: 'The metal–insulator transitions of VO_2: a band theoretical approach', *Ann. Phys.*, 2002, **11**, p. 650

[5] Case F.C.: 'Influence of ion beam parameters on the electrical and optical properties of ion-assisted reactively evaporated vanadium dioxide thin films', *Vac. Sci. Technol.*, 1987, **A5**, p. 1762

[6] Barker A.S., Verleur H.W., Guggenheim H.J.: 'Infrared optical properties of vanadium dioxide above and below transition temperature', *Phys. Rev. Lett.*, 1966, **17**, p. 1286

[7] Li Y., Ji S., Gao Y., Luo H., Kanehira M.: 'Core-shell VO_2@ TiO_2 nanorods that combine thermochromic and photocatalytic properties for application as energy-saving smart coatings', Scientific reports, 2013, vol. 3

[8] Li W., Ji S., Qian K., Jin P.: 'Preparation and characterization of VO_2(M)-SnO_2 thermochromic films for application as energy-saving smart coatings', *J. Colloid Interface Sci.*, 2015, **456**, p. 166

[9] Karimov K.S., Tahir M.M., Saleem M., Chani M.T.S., Niaz A.K.: 'Temperature sensor based on composite film of vanadium complex (VO_2(3-fl)) and CNT', *J. Semicond.*, 2015, **36**

[10] Jiang L., Carr W.N.: 'Vanadium dioxide thin films for thermo-optical switching applications'. MRS Proc., 2003, vol. 785

[11] Jiang L., Carr W.N.: 'Design, fabrication and testing of a micromachined thermo-optical light modulator based on a vanadium dioxide array', *J. Micromech. Microeng.*, 2004, **14**, p. 833

[12] Paone A., Joly M., Sanjines R., Romanyuk A., Scartezzini J.L., Schüler A.: 'Thermochromic films of VO_2:W for smart solar energy applications'. SPIE Solar Energy Technology, 2009, pp. 74100F–74100F

[13] Lu Y., Zhou S., Gu G., Wu L.: 'Preparation of transparent, hard thermochromic polysiloxane/tungsten-doped vanadium dioxide nanocomposite coatings at ambient temperature', *Thin Solid Films*, 2013, **534**, p. 231

[14] Zhang Y., Zhang J., Zhang X., Huang C., Zhong Y., Deng Y.: 'The additives W, Mo, Sn and Fe for promoting the formation of VO_2 (M) and its optical switching properties', *Mater. Lett.*, 2013, **92**, p. 61

[15] Liu S.J., Fang H.W., Su Y.T., Hsieh J.H.: 'Metal–insulator transition characteristics of Mo- and Mn-doped VO_2 films fabricated by magnetron cosputtering technique', *Jpn. J. Appl. Phys.*, 2014, **53**, p. 063201

[16] Batista C., Ribeiro R.M., Teixeira V.: 'Synthesis and characterization of VO_2-based thermochromic thin films for energy-efficient windows', *Nanoscale Res. Lett.*, 2011, **6**, p. 1

[17] Mlyuka N., Niklasson G., Granqvist C.G.: 'Mg doping of thermochromic VO_2 films enhances the optical transmittance and decreases the metal–insulator transition temperature', *Appl. Phys. Lett.*, 2009, **95**, p. 171909

[18] Li S.Y., Mlyuka N.R., Primetzhofer D., *ET AL.*: 'Bandgap widening in thermochromic Mg-doped VO_2 thin films: quantitative data based on optical absorption', *Appl. Phys. Lett.*, 2013, **103**, p. 161907

[19] Shen N., Chen S., Chen Z., *ET AL.*: 'The synthesis and performance of Zr-doped and W–Zr-codoped VO_2 nanoparticles and derived flexible foils', *J. Mater. Chem. A*, 2014, **2**, p. 15087
[20] Ramírez J.G., Sharoni A., Dubi Y., Gomez M.E., Schuller I.K.: 'First-order reversal curve measurements of the metal-insulator transition in VO_2: signatures of persistent metallic domains', *Phys. Rev.*, 2009, **B79**, p. 235110
[21] Zhang Y., Huang W.X., Shi Q.W., Song L.W., Xu Y.J.: 'Thermal modulation behavior inside the hysteresis loop of W–Mo co-doping vanadium dioxide film', *J. Inorg. Mater.*, 2013, **28**, p. 497
[22] Nishikawa M., Nakajima T., Kumagai T., Okutani T., Tsuchiya T.: 'Adjustment of thermal hysteresis in epitaxial VO_2 films by doping metal ions', *J. Ceram. Soc. Jpn*, 2011, **119**, p. 577
[23] Warwick M.E., Ridley I., Binions R.: 'The effect of variation in the transition hysteresis width and gradient in thermochromic glazing systems', *Sol. Energy Mater. Sol. Cells*, 2015, **140**, p. 253
[24] Lopez R., Boatner L.A., Haynes T.E.: 'Enhanced hysteresis in the semiconductor-to-metal phase transition of VO_2 precipitates formed in SiO_2 by ion implantation', *Appl. Phys. Lett.*, 2001, **79**, p. 3161
[25] Dai J., Wang X., He S., Huang Y., Yi X.: 'Low temperature fabrication of VO_x thin films for uncooled IR detectors by direct current reactive magnetron sputtering method', *Infrared Phys. Technol.*, 2008, **51**, p. 287
[26] Wang N., Magdassi S., Mandler D., Long Y.: 'Simple sol–gel process and one-step annealing of vanadium dioxide thin films: synthesis and thermochromic properties', *Thin Solid Films*, 2013, **534**, p. 594
[27] Warwick M.E., Binions R.: 'Chemical vapour deposition of thermochromic vanadium dioxide thin films for energy efficient glazing', *J. Solid State Chem.*, 2014, **214**, p. 53
[28] Outkina E.A., Vorobyova A.I., Khodin A.A.: 'Formation and properties of thin-film composites vanadium oxide/porous anodic aluminum oxide', *Russ. Microelectron.*, 2010, **39**, p. 273
[29] Xu M., Wang J., Li L., Wu C., Zhao Y., Zuo H.: 'Preparation of thermochromic vanadium dioxide thin films by pulsed-magnetron sputtering', *Appl. Mech. Mater.*, 2013, **377**, p. 227
[30] Chae B.G., Youn D.H., Kim H.T., Maeng S.Y., Kang K.Y.: 'Fabrication and electrical properties of pure VO_2 phase films', 2003, arXiv preprint cond-mat/0311616
[31] Nag J., Haglund R.F.: 'Synthesis of vanadium dioxide thin films and nanoparticles', *Phys. Condens. Matter*, 2008, **20**, p. 1
[32] Vinichenko D.A., Zlomanov V.P., Vasil'ev V.A., Seregin D.S., Berezina O.Y.: 'Synthesis of vanadium dioxide films by a modified sol–gel process', *Inorg. Mater.*, 2011, **47**, p. 279
[33] Khan G.R., Khan R.A.: 'Ergonomic synthesis suitable for industrial production of silver-festooned zinc oxide nanorods', *Int. J. Nanosci.*, 2015, doi: 10.1142/S0219581X15500180
[34] Kürüm U., Yaglioglu H.G., Küçüköz B., *ET AL.*: 'Excited state dynamics of nanocrystalline VO_2 with white light continuum time resolved spectroscopy', *Opt. Commun.*, 2014, **333**, p. 109
[35] Caruthers E., Kleinman L.: 'Energy bands of semiconducting VO_2', *Phys. Rev. B*, 1973, **7**, p. 3760
[36] Ghobad N.: 'Band gap determination using absorption spectrum fitting procedure', *Int. Nano Lett.*, 2013, **3**, p. 2
[37] Wentzcovitch R.M., Schulz W.W., Allen P.B.: 'VO_2: Peierls or Mott-Hubbard? A view from band theory', *Phys. Rev. Lett.*, 1994, **72**, p. 3389
[38] Liebsch A., Ishida H., Bihlmayer G.: 'Coulomb correlations and orbital polarization in the metal-insulator transition of VO_2', *Phys. Rev. B*, 2005, **71**, p. 085109
[39] Biermann S., Poteryaev A., Lichtenstein A.I., Georges A.: 'Dynamical singlets and correlation-assisted Peierls transition in VO_2', *Phys. Rev. Lett.*, 2005, **94**, p. 026404
[40] Haverkort M.W., Hu Z., Tanaka A., *ET AL.*: 'Orbital-assisted metal-insulator transition in VO_2', *Phys. Rev. Lett.*, 2005, **95**, p. 196404
[41] Qazilbash M.M., Burch K.S., Whisler D., *ET AL.*: 'Correlated metallic state of vanadium dioxide', *Phys. Rev. B*, 2006, **74**, p. 205118
[42] Wei J., Wang Z., Chen W., Cobden H.: 'New aspects of the metal–insulator transition in single-domain vanadium dioxide nanobeams', *Nat. Nanotechnol.*, 2009, **4**, p. 420
[43] Eyert V.: 'VO_2: a novel view from band theory', *Phys. Rev. Lett.*, 2011, **107**, p. 016401
[44] Wang C.X., Yang G.W.: 'Thermodynamics of metastable phase nucleation at the nanoscale', *Mater. Sci. Eng. R*, 2005, **49**, p. 157
[45] Narayan J., Bhosle V.M.P.: 'Phase transition and critical issues in structure–property correlations of vanadium oxide', *Appl. Phys.*, 2006, **100**, p. 103524

doi: 10.1049/mnl.2015.0213